

PACS numbers: 42.55.Px; 42.60.Jf
DOI: 10.1070/QE2001v031n03ABEH001921

Competition between spatial Fourier modes in a wide-aperture vertical-cavity surface-emitting semiconductor laser

N A Loiko, I V Babushkin

***Abstract*. Formation of periodic structures in a transverse cross section of the emission of vertical-cavity surface-emitting semiconductor lasers is studied. It is shown that spatial Fourier modes of the emission are selected not only through the well-known mechanism related to the gain dispersion, but also through the dependence of the reflection coefficient of Bragg mirrors on the angle of incidence of the wave. This mechanism gives rise to the selection of standing transverse waves, whose direction is determined by the polarisation vector of the radiation. The effect of the laser cavity symmetry with respect to the active layer on the mode selection is studied.**

Keywords: *vertical-cavity surface-emitting semiconductor laser, spatial Fourier modes, Bragg mirrors, spatial structures.*

Vertical-cavity surface-emitting lasers (VCSELs) are promising light sources for optical data processing and optical fibre communication systems owing to the advantages brought by their geometry: compactness, a circularly symmetric beam profile, the possibility of being densely packed in a surface-emitting system, and single-mode lasing [1]. A special feature of these lasers is a large Fresnel number, which can reach a few tens without any need to use curved mirrors, as in the case of lasers with long cavities [2].

In their transverse beam sections, wide-aperture lasers with plane cavities can form periodic structures, such as travelling or standing waves, optical vortex-like localised structures, or spatial solitons [3 – 7]. This makes VCSELs ideal candidates for studying these processes, which is important for diversifying their applications and understanding the fundamental aspects of spatial structure formation in dissipative systems.

Theoretical analysis of lasers with large Fresnel numbers is usually based on the semiclassical description of the lasing process with the help the Maxwell – Bloch equations for the field and medium characteristics that are averaged over the longitudinal cavity dimension [3 – 5]. In this model, the discrimination of spatial Fourier modes (oblique cavity waves) is caused by the dispersion of the medium gain and is determined by the detuning, $\delta = \omega_a - \omega_c$ of the transition frequency ω_a of the medium from the cavity frequency ω_c. An inhomogeneous radiation profile can be formed only if $\delta > 0$, when travelling transverse waves appear.

In this work, we show that the dependence of the reflection coefficient of Bragg mirrors on the angle of incidence of the wave also causes the selection of spatial field harmonics in the emission of a VCSEL. The inclusion of this mechanism in the theoretical treatment gives rise to the selection of transverse standing waves whose direction depends on the polarisation of the radiation. The resulting structures are then similar to those observed experimentally [8].

The mode selection process can become more complex if we take into account the polarisation of the emission, characteristic of this type of lasers due to their weak anisotropy [9, 10]. In this work, however, we will consider a laser operating near the lasing threshold, when the radiation with a certain linear polarisation is stable to orthogonally polarised perturbations (the scalar case).

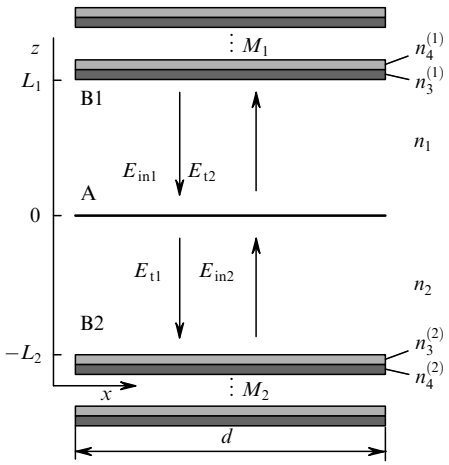

Figure 1. Model of the vertical-cavity laser: (A) thin active layer of thickness l, (B1, B2) Bragg reflectors at distances L_1 and L_2 from the active layer. Each of the Bragg reflectors consists of M_i ($i = 1, 2$) periods, which, in turn, consist of quarter-wave layers with $n_3^{(i)}$ and $n_4^{(i)}$. The spaces between the Bragg reflectors and the active medium are filled with media whose refractive indices are n_1 and n_2, respectively. E_{in1} and E_{in2} are the fields incident on the active layer; E_{t1} and E_{t2} are the transmitted fields.

In our model, the VCSEL is a thin-film system [11, 12] with the radiation consecutively passing through individual

N A Loiko, I V Babushkin B N Stepanov Institute of Physics, National Academy of Sciences of Belarus, prosp. F.Skoriny 70, 220072 Minsk, Belarus

Received 28 July 2000; revision received 6 December 2000
Kvantovaya Elektronika **31** (3) 221 – 226 (2001)
Translated by I V Bargatin

elements of the resonator (Fig. 1). We assume that the active layer of thickness l is located between two linear media with refractive indices n_1 and n_2. The cavity is formed by the upper and lower Bragg reflectors, which consist of M_i pairs of alternating layers with refractive indices $n_3^{(i)}$ and $n_4^{(i)}$ ($i = 1, 2$). In many devices used, the thickness l of the active layeris smaller than the radiation wavelength. In this case, we can neglect the diffraction in the active layer and represent the field inside it as the sum of the two incident waves $E_{\rm in1}$ and $E_{\rm in2}$ and the secondary wave produced by the polarisation of the medium [13]:

$$E(t, \boldsymbol{r}_\perp) = E_{\rm in1}(t, \boldsymbol{r}_\perp) + E_{\rm in2}(t, \boldsymbol{r}_\perp) + \frac{2\pi {\rm i}\omega l}{c} P(t, \boldsymbol{r}_\perp). \quad (1)$$

Here, E ($E_{\rm in}$) and P are the slowly varying (on the wavelength scale) amplitudes of the electromagnetic fields and polarisation of the active medium, respectively; ω is the wavelength of the emission, usually coinciding with the cavity frequency $\omega_{\rm c}$; $\boldsymbol{r}_\perp = (x, y)$ is the coordinate in the plane of the transverse cross section (the active layer). The fields $E_{\rm t1}$ and $E_{\rm t2}$ transmitted by the active layer are related to the incident fields by

$$E_{\rm t1,2}(t, \boldsymbol{r}_\perp) = E_{\rm in1,2}(t, \boldsymbol{r}_\perp) + \frac{2\pi {\rm i}\omega l}{c} P(t, \boldsymbol{r}_\perp). \quad (2)$$

The propagation of the radiation inside the cavity can be written in the operator form:

$$E_{\rm in1,2}(t, \boldsymbol{r}_\perp) = \hat{F}_{1,2} E_{\rm t1,2}(t, \boldsymbol{r}_\perp), \quad (3)$$

where

$$\hat{F}_{1,2} = \rho_{1,2} \exp({\rm i}2kL_{1,2}) \exp\left({\rm i}\frac{\Delta_\perp}{k} L_{1,2}\right) \hat{R}_{1,2} \quad (4)$$

are the propagators, $\rho_{1,2}$ are the losses due to the passage of radiation through the linear (in the general case, absorbing) medium between the active layer and the reflector; $L_{1,2}$ are the thicknesses of the linear layers at the two sides of the active medium; and $\Delta_\perp$ is the transverse part of the Laplacian.

The first parts of the propagation operators, containing exponents, describe the light propagation in the linear medium between the active layer and the mirrors. It is a formal solution of the equation of diffraction in the paraxial approximation. Note that $\Delta_\perp$ acts in the $\boldsymbol{k}_\perp$ space so that $\Delta_\perp \propto |\boldsymbol{k}_\perp|^2$, where

$$\boldsymbol{k}_\perp = \begin{pmatrix} k_x \\ k_y \end{pmatrix}$$

is the transverse component of the total wave vector $\boldsymbol{k}$ of the light field, and $k = \omega/c = 2\pi/\lambda$ is its modulus.

Operators $\hat{R}_{1,2}$ are defined in the $\boldsymbol{k}_\perp$-space as the reflection coefficients $R_{1,2}$ of the Bragg mirrors for each plane wave with the vector $\boldsymbol{k}_\perp$. They can be calculated by expanding the field $E(\boldsymbol{k}_\perp)$ in TE and TM components, for which the reflection coefficients of thin-film systems are known [14], and then changing back to the (x, y) basis [15]. Assuming that the radiation field is polarised along the x axis, we obtain

$$R_i(\boldsymbol{k}_\perp) = r_{s,i}(\boldsymbol{k}_\perp)\varepsilon_{sx}^2 - r_{p,i}(\boldsymbol{k}_\perp)\varepsilon_{sy}^2, \quad (5)$$

where $\varepsilon_{sx} = -k_y/k_\perp$, $\varepsilon_{sy} = k_x/k_\perp$; r_s and r_p are the reflection coefficients for the TE and TM modes, respectively, and $i = 1, 2$.

Combining relations (1)–(3), one can easily derive the recurrent relation expressing the radiation field inside the active medium in terms of the cavity round-trip time $\tau = \tau_1 + \tau_2$:

$$E(t, \boldsymbol{r}_\perp) = \hat{F}_1\hat{F}_2 E(t-\tau, \boldsymbol{r}_\perp) + \frac{2\pi {\rm i}\omega l}{c}[P(t, \boldsymbol{r}_\perp)$$

$$+\hat{F}_1 P(t-\tau_1, \boldsymbol{r}_\perp) + \hat{F}_2 P(t-\tau_2, \boldsymbol{r}_\perp) + \hat{F}_1\hat{F}_2 P(t-\tau, \boldsymbol{r}_\perp)]. \quad (6)$$

In the derivation of Eqn (6), we used the fact that operators $\hat{F}_1$ and $\hat{F}_2$ commute, which can be easily proven in the considered case (i.e., the specific sequence in which the light passes through different parts of the cavity is insignificant). The time delays τ_1 and τ_2 due to the finite time of the light transit through different parts of the cavity are determined by the effective lengths of these parts, including the penetration depth of the radiation into the Bragg reflectors [16].

The response of the active semiconductor medium is described by the Bloch equations for the polarisation and the charge carrier density for each optical transition from the conduction band to the valence band, which is characterised by the wave vector [17]. Using rather general assumptions, the equations for the total polarisations and the carrier density can be reduced to equations similar to those describing a two-level medium. The parameters of this medium depend on the carrier density and the temperature [18]. We will assume that, near the lasing threshold, the susceptibility of the medium linearly depends on the carrier density at the maximum of the gain profile, and that the remaining parameters, which determine the Lorentzian shape of the gain profile, are virtually constant. Our starting point will be the two-level Bloch equations, which, in the limit of a broad gain profile, reduce to the phenomenological rate equations, which adequately describe many lasing properties of semiconductor lasers. This considerably simplifies our analysis and numerical experiment while preserving the main features of the process under study and offering an insight into the roles of the gain dispersion and losses in the formation of the spatial structure of the emission.

The Bloch equations for the polarisation P and the carrier density N have the form

$$\frac{{\rm d}P}{{\rm d}t} = -\left(\frac{1}{T_2} + {\rm i}\delta\right)P - \frac{|\boldsymbol{d}|^2}{3\hbar}{\rm i}(N - N_0)E,$$

$$\frac{{\rm d}N}{{\rm d}t} = -\frac{N - J}{T_1} - \frac{\rm i}{2\hbar}(E^*P - EP^*), \quad (7)$$

where T_1 and T_2 are the relaxation times of the carrier density and the polarisation, respectively, N_0 is the carrier density necessary to reach the state of transparency, $|\boldsymbol{d}|$ is the modulus of the transition dipole moment, and J is the pump parameter.

The conditions for each of the transverse field harmonics $\boldsymbol{k}_\perp = (k_x, k_y)$ of the cavity are different, and so are the shifts of their frequencies from the transition frequency of the active medium and from the cavity frequency for the zero mode with $\boldsymbol{k}_\perp = 0$. Therefore, we will look for the solution

of system (6), (7) by expanding the field $E(t, \boldsymbol{r}_\perp)$ and the polarisation $P(t, \boldsymbol{r}_\perp)$ in the spatial harmonics:

$$E(t,\boldsymbol{r}_\perp) = \int E(t,\boldsymbol{k}_\perp)\exp(-\mathrm{i}\,\boldsymbol{r}_\perp\boldsymbol{k}_\perp)\mathrm{d}\boldsymbol{k}_\perp\,,$$

$$P(t,\boldsymbol{r}_\perp) = \int P(t,\boldsymbol{k}_\perp)\exp(-\mathrm{i}\,\boldsymbol{r}_\perp\boldsymbol{k}_\perp)\mathrm{d}\boldsymbol{k}_\perp\,.$$

We will assume that relatively fast temporal variations on the scale of the cavity round-trip time are due exclusively to the adjustment of the radiation phase, whereas the amplitudes of the spatial harmonics vary relatively slowly. Then, these harmonics can be treated as quasi-plane waves:

$$\begin{aligned} E(t,\boldsymbol{k}_\perp) &= e(t,\boldsymbol{k}_\perp)\exp\{-\mathrm{i}[\Omega(\boldsymbol{k}_\perp)t - \boldsymbol{k}_\perp\boldsymbol{r}_\perp]\},\\ P(t,\boldsymbol{k}_\perp) &= p(t,\boldsymbol{k}_\perp)\exp\{-\mathrm{i}[\Omega(\boldsymbol{k}_\perp)t - \boldsymbol{k}_\perp\boldsymbol{r}_\perp]\}. \end{aligned} \tag{8}$$

Considering the case of a stationary state, i.e., time-independent amplitudes e and p, we insert Eqn (8) into Eqns (6) and (7), arriving at

$$\begin{aligned} 1 &= \tilde{r}_1(\boldsymbol{k}_\perp)\tilde{r}_2(\boldsymbol{k}_\perp) + \frac{2\pi\omega l\,|d|^2 T_2}{3c\hbar}\mathscr{L}_\omega(\boldsymbol{k}_\perp)\{(1+\mathrm{i}\alpha)\\ &\quad\times D[1+\tilde{r}_1(\boldsymbol{k}_\perp)\tilde{r}_2(\boldsymbol{k}_\perp)+\tilde{r}_1(\boldsymbol{k}_\perp)+\tilde{r}_2(\boldsymbol{k}_\perp)]\\ &\quad-\mathrm{i}\alpha D_0[1+r_1(0)r_2(0)+r_1(0)+r_2(0)]\},\\ p &= -\frac{|d|^2 T_2}{3\hbar}\mathscr{L}_\omega(\boldsymbol{k}_\perp)(\mathrm{i}-\alpha)De, \qquad (9)\\ e^2 &= \frac{3\hbar^2(J-D)}{|d|^2 T_1 T_2 L_\omega D}. \end{aligned}$$

Here, $D = N - N_0$; J is the appropriately redefined pump parameter; $\mathscr{L}_\omega(\boldsymbol{k}_\perp) = 1/\{1+[(\delta-\Omega(\boldsymbol{k}_\perp)T_2]^2\}$ is the Lorentzian gain profile; $\tilde{r}_j(\boldsymbol{k}_\perp) = r_j(\boldsymbol{k}_\perp)\exp[\mathrm{i}\theta_j(\boldsymbol{k}_\perp)]$; $r_i(\boldsymbol{k}_\perp) = |R_i|$ are the moduli of the reflection coefficients of the Bragg structures; and $s_i(\boldsymbol{k}_\perp)$ are their phases, which enter the expressions for the total phases: $\theta_j(\boldsymbol{k}_\perp) = s_i(\boldsymbol{k}_\perp) + 2kL_i - |\boldsymbol{k}_\perp|^2 L_i/k + \Omega(\boldsymbol{k}_\perp)\tau_i$. The quantity α characterises the relative variation in the refractive index and the gain caused by a variation in the number of carriers. In contrast to the case of a two-level model, where $\alpha = -\delta T_2$, in semiconductors this parameter is independent of the sign of the frequency detuning from the maximum of the gain profile, and remains nonzero at $\delta = 0$. We use this fact in the following discussion.

The last term in the first equation of system (9) was introduced to remove the frequency shift of the zero harmonic ($\boldsymbol{k}_\perp = 0$) at its lasing threshold ($D = D_0$), which is caused by the variation in the refractive index of the active medium produced by the change in the number of carriers. A similar term should also be added to equation (6). When the active layer is located at an antinode of the cavity's standing wave, we have $s_i(0) + 2kL_i = j_i\pi$, where j_i integers. Assuming that the resonance conditions are satisfied, i.e. $j_1 + j_2$ is an integer number and, accordingly, $\Omega(0) = 0$, we obtain

$$D_0 = \frac{3c\hbar[1-r_1(0)r_2(0)]}{2\pi\omega l|d|^2 T_2\mathscr{L}_\omega(0)[1+r_1(0)r_2(0)+r_1(0)+r_2(0)]}. \tag{10}$$

The values of D found from Eqn (9) determine the lasing threshold for each transverse mode. Obviously, the modes with the minimum D will be the first to start lasing, and if the transverse wave vectors of these harmonics are nonzero, spatial structures will appear.

Consider first the simplest case when the reflection coefficients of the mirrors are independent of the angle of incidence. Then, the relative excitation threshold of a spatial Fourier mode with a given wave vector is determined by its frequency detuning from the maximum of the gain profile:

$$\frac{D}{D_0} = \frac{\mathscr{L}_\omega(0)}{\mathscr{L}_\omega(\boldsymbol{k}_\perp)} = \frac{\{[\delta-\Omega(\boldsymbol{k}_\perp)]T_2\}^2+1}{(\delta T_2)^2+1}. \tag{11}$$

Expression (11) yields the well-known result [2–5] that, in the case of a positive detuning, $\delta > 0$, the minimum excitation threshold corresponds to the harmonic with $\Omega(\boldsymbol{k}_\perp) = \delta$. This mechanism of spatial mode selection is related to the gain dispersion. The lasing threshold of each mode then depends on $|\boldsymbol{k}_\perp|$ only, i.e. there is no preferred direction for the resulting spatial structures. The gain threshold $\mu = J/D_0$ of every mode is shown for this case by the dash-dot curve in Fig. 2 (the $k_x = 0$ section is shown).

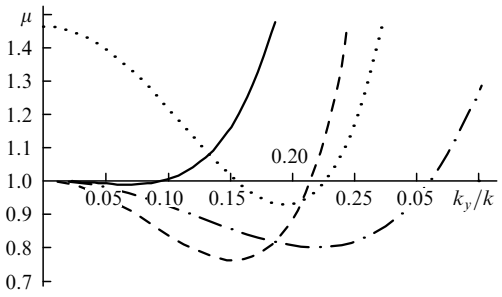

Figure 2. Dependence of the gain threshold μ on the parameter k_y/k, describing the slope of the spatial mode to the cavity axis. The curves are for the $k_x = 0$ section and parameter $\delta T_2 = 0.5$ with ordinary (non-Bragg) mirrors with the same reflection coefficient (dash-dot curve), 0.1 (solid curved), 0.5 (dashed curve), and 0.5 with an asymmetric cavity (dotted curve). The remaining parameters were $\alpha = 3$, $\kappa = T_1\tau^{-1}[1-r_1(0)r_2(0)] = 300$, $L_1 = L_2 = \lambda$, $n_1 = n_2 = 3.2$, $n_3^{(1)} = n_3^{(2)} = 3.0$, $n_4^{(1)} = n_4^{(2)} = 3.56$, $n_l^{(1)} = n_l^{(2)} = 3.2$, and $M_1 = M_2 = 16$. All curves are symmetric with respect to the origin $k_y = 0$.

In the case of a negative detuning, the emission profile should be homogeneous near the lasing threshold. Assuming that the susceptibility of the active medium is frequency-independent, the selection is determined exclusively by the dependence of the reflection coefficients of the Bragg mirrors on $\boldsymbol{k}_\perp$. Therefore, we have

$$\frac{D}{D_0} = \frac{[1-\tilde{r}_1(\boldsymbol{k}_\perp)\tilde{r}_2(\boldsymbol{k}_\perp)][1+r_1(0)r_2(0)+r_1(0)+r_2(0)]}{[1-r_1(0)r_2(0)][1+\tilde{r}_1(\boldsymbol{k}_\perp)\tilde{r}_2(\boldsymbol{k}_\perp)]+\tilde{r}_1(\boldsymbol{k}_\perp)+\tilde{r}_1(\boldsymbol{k}_\perp)]}. \tag{12}$$

As is well known, the reflection coefficient $r_i(\boldsymbol{k}_\perp)$ is an anisotropic function in the case of linearly polarised light. The harmonics whose wave vector is perpendicular to the polarisation vector, $k_x = 0$, $k_y \neq 0$, have the best reflection conditions (Figs 3a,b). This anisotropy gives rise to minima of the lasing threshold at nonzero spatial frequencies. In accordance with the reflection coefficients, these lasing thres-

hold minima correspond to the harmonics that are perpendicular to the radiation polarisation (Figs 3c,d). As compared to previous case of the gain dispersion mechanism, the mode selection near the lasing threshold is softer, i.e, the minima are much shallower.

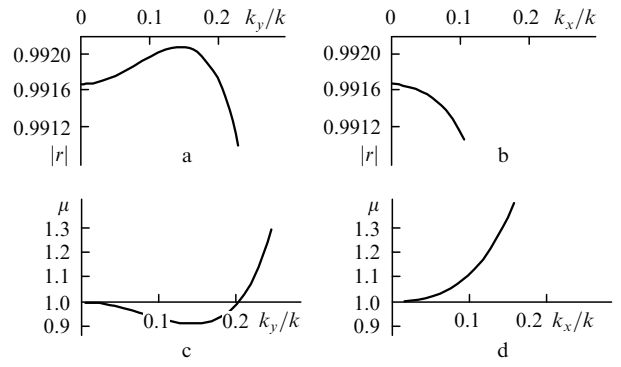

Figure 3. Angular dependences of the reflection coefficient of the Bragg mirrors (a, b) and the threshold pumping current in the absence of the Lorentzian gain dispersion (c, d) in sections $k_x = 0$ (a, c) and $k_y = 0$ (b, d). The curves are symmetric with respect to the origin $k_y = 0$.

The interplay between the two mechanisms of the spatial harmonics selection can be either constructive, with both mechanisms enhancing each other, or destructive. Fig. 2 shows the dependence of the gain threshold for the spatial harmonics of the $k_x = 0$ section (where the lasing threshold reaches its absolute minimum) for various parameters of the system. In the case of the exact resonance ($\delta = 0$) or a negative detuning, the minima due to the Bragg mechanism of the spatial mode selection disappear if the gain profile is sufficiently narrow. In the case of a broad gain profile, they merely shift towards $k_y = 0$ and become shallower (Fig. 2, solid curve).

The dashed curve in Fig. 2 shows an example of the constructive interplay in the case of $\delta > 0$. The lasing threshold minimum deepens and shifts towards larger k_y, where the maximum of the mirror reflection coefficients is located when the Bragg dispersion mechanism is neglected (see Fig. 2, dash-dot line). Note that the lasing threshold for the zero spatial harmonic remains unchanged. Fig. 4 shows

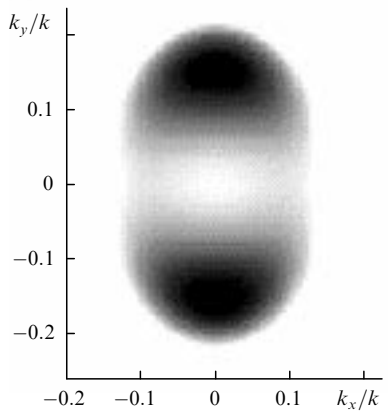

Figure 4. Angular dependence of the threshold pumping current in the (k_x, k_y) plane with the parameters as in Fig. 2 and $\delta T_2 = 0.5$.

the complete spatial dependence of the lasing threshold in this case. One can see that the strong anisotropy that is characteristic of the Bragg mechanism remains when both mechanisms are active, whereas the depth of the minima and their positions in the (k_x, k_y) plane are mainly determined by the dispersion mechanism. Thus, under the combined influence of the two mechanisms, the anisotropy introduced by the Bragg mirrors is enhanced by the dispersion.

Now consider how the position of the active layer in the cavity affects the lasing threshold of transverse modes. The analysis of the system of equations (9) shows that, if the reflection coefficients of the two Bragg structures are the same, a small displacement of the active layer from the antinode of the cavity's standing wave changes only amplitudes, proportionally increasing the lasing threshold of all harmonics. A stronger symmetry violation, which can be produced, for example, by introducing an absorbing layer in one part of the cavity, gives rise to a phase mismatch and shifts the frequencies of all spatial harmonics. As a result, the effective detuning $\delta - \Omega(\boldsymbol{k}_\perp)$ of a sideband mode can become smaller than the effective detuning of the zero harmonic even when $\delta < 0$. This mode will have the minimum lasing threshold. In the case of a positive δ, the minima of the function $D(\boldsymbol{k}_\perp)$ become more pronounced (see the dash-dot and dotted curves in Fig. 2), while the threshold for the zero mode rises because it no longer experiences the best lasing conditions.

To simplify the numerical integration of equations (1)–(7), we will use the hierarchy of characteristic times that is typical for a system formed by a semiconductor medium and a microcavity. In particular, the characteristic cavity round-trip time is $\tau \sim 10^{-14}$ s, the relaxation time of the polarisation is $T_2 \sim 10^{-12}$ s, and the relaxation time of the carrier population is $T_1 \sim 10^{-9}$ s.

To exclude the time scale of the cavity round-trip from the equations, we evoke the above assumption that the field amplitude changes little over time τ. Then, $e(t+\tau) = e(t) + \tau \mathrm{d}e(t)/\mathrm{d}t$, and the difference equation (6) reduces to a differential one.

Assuming also that the short relaxation time of the polarisation of a semiconductor medium makes it possible to use the quasi-stationary approximation for each of its spatial components, we replace the equation for the polarisation by relation

$$P = -\frac{|\boldsymbol{d}|^2 T_2}{3\hbar}(\mathrm{i} - \alpha)\,\hat{\mathscr{L}}_\omega(DE). \tag{13}$$

Within these approximations, the equations for the normalised amplitude of the emission field, $E \to (|\boldsymbol{d}|^2 \times T_2/3\hbar^2)^{1/2}E$, and the normalised carrier density, $D \to D/D_0$, take the form

$$\frac{\mathrm{d}E(t,\boldsymbol{r}_\perp)}{\mathrm{d}t} = -\kappa\hat{M}E(t,\boldsymbol{r}_\perp) - \mathrm{i}\hat{\Omega}E(t,\boldsymbol{r}_\perp) - \mathrm{i}\kappa\alpha E(t,\boldsymbol{r}_\perp)$$
$$+ \kappa(1 + \mathrm{i}\alpha)\hat{G}(DE(t,\boldsymbol{r}_\perp)), \tag{14}$$
$$\frac{\mathrm{d}D(t,\boldsymbol{r}_\perp)}{\mathrm{d}t} = -D(t,\boldsymbol{r}_\perp) + \mu - \mathrm{Im}\big[(\mathrm{i} - \alpha)E^*(t,\boldsymbol{r}_\perp)$$
$$\times \hat{\mathscr{L}}_\omega\big(D(t,\boldsymbol{r}_\perp)E(t,\boldsymbol{r}_\perp)\big)\big].$$

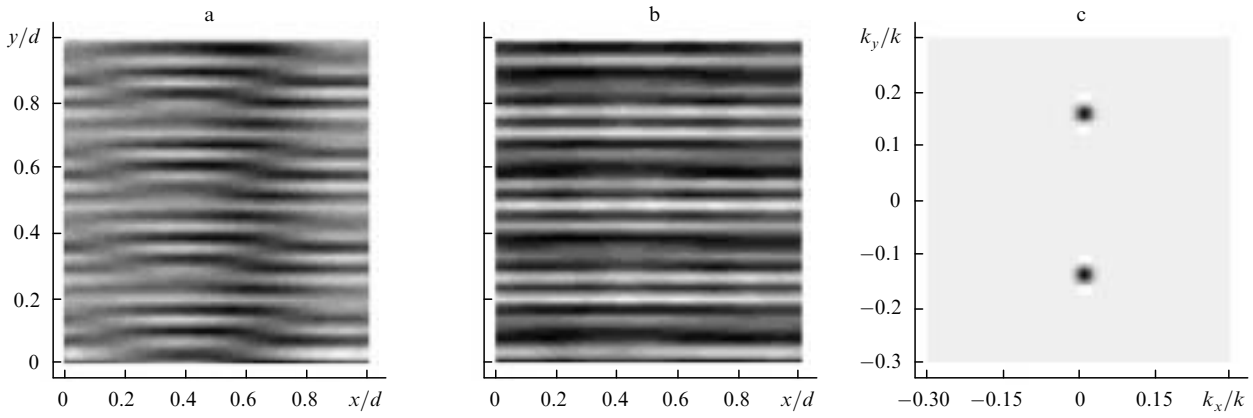

Figure 5. Stripes calculated by the numerical integration of the system in the near-field zone at a fixed time instant (a), as well as the near- (b) and far-field (c) structures averaged over a time interval of $t/T_1 \sim 10$. The parameters are as in Fig. 4; $\mu = 0.8$.

Here, time t is normalised by the relaxation time T_1 of the carrier density and $\kappa = T_1\tau^{-1}[1 - r_1(0)r_2(0)]$.

The operators entering system of equations (14) act as follows:

$$\hat{\Omega} \propto \Omega(\boldsymbol{k}_\perp), \quad \hat{M} \propto \frac{1 - \tilde{r}_1(\boldsymbol{k}_\perp)\tilde{r}_2(\boldsymbol{k}_\perp)}{1 - r_1(0)r_2(0)}, \qquad (15)$$

$$\hat{G} \propto \frac{1 + \tilde{r}_1(\boldsymbol{k}_\perp) + \tilde{r}_2(\boldsymbol{k}_\perp) + \tilde{r}_1(\boldsymbol{k}_\perp)\tilde{r}_2(\boldsymbol{k}_\perp)}{1 + r_1(0) + r_2(0) + r_1(0)r_2(0)} \frac{\mathscr{L}_\omega(\boldsymbol{k}_\perp)}{\mathscr{L}_\omega(0)}.$$

The frequencies $\Omega(\boldsymbol{k}_\perp)$ are assumed to coincide with their steady-state values; $\hat{\mathscr{L}}_\omega \propto \mathscr{L}_\omega(\boldsymbol{k}_\perp)$.

If the spatial effects are neglected, system of equations (14) for a single mode with $\boldsymbol{k}_\perp = 0$ reduces to the ordinary system of rate equations, widely used to describe the emission dynamics. When all spatial modes are taken into account, the intermodal competition considered above gives rise to a minimum of the threshold at $\boldsymbol{k}_\perp \neq 0$. The spatially homogeneous state ($E = 0$, $D = \mu$) then yields its stability to a state with $\boldsymbol{k}_\perp \neq 0$. In the immediate vicinity of the lasing threshold, the anisotropy of the system should give rise to the transverse waves whose $\boldsymbol{k}_\perp$ corresponds to the lasing threshold minimum [19].

For the numerical integration of system (14), we used the Runge–Kutta method, performing the fast Fourier transform at each integration step in order to calculate the action of the operators that appear in the right-hand side of Eqns (14). We assumed periodic boundary conditions.

For a pump intensity near the lasing threshold, the system reached its steady state after some transition process, and formed the spatial structures shown in the near field in Fig. 5a. The patterns averaged over the largest oscillation period, $t \sim 10$, are shown in Figs 5b and 5c (the near- and far-field zones). These structures are standing waves, whose period corresponds to the modes having the minimum lasing threshold. The orientation of these structures coincides with the polarisation of the emission, in agreement with the experimental data of Ref. [8].

The stripes shown in Fig. 5a exhibit small-amplitude steady-state oscillations, shown in Figs 6a and 6b for a single point of the cross section. One can see that these oscillations have three characteristic frequencies. The oscillations with a period of $\sim 10^{-1}$ are due to the beating of spatial modes $\boldsymbol{k}_\perp$ with different frequencies $\Omega(\boldsymbol{k}_\perp)$. This beating is virtually absent in the dynamics of D. Oscillations with periods of ~ 1 and ~ 10 describe the longitudinal and transverse oscillations of the entire spatial structure. The period of ~ 1 is close to the period of relaxation oscillations. Note that the intensity peaks in the far-field zone (Fig. 5c) oscillate with this period too, with the two peaks having opposite phases. Interestingly, a weak longitudinal and transverse modulation of the spatial structures was also observed in experiment.

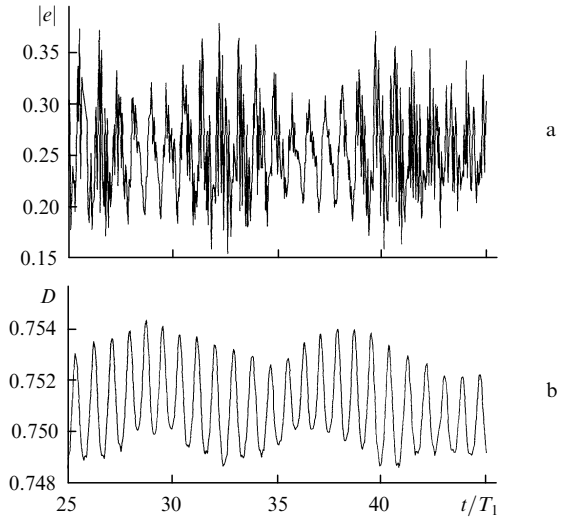

Figure 6. Fig. 6. Steady-state temporal dynamics of the field intensity (a) and carrier density (b) in a point of the transverse structure shown in Fig. 5.

Ref. [8] does not provide the values of $\boldsymbol{k}_\perp$ for the resulting spatial structures. However, its authors have shown that in the case of a varying cavity length (which is equivalent to a variation in δ), at $\delta > 0$ the frequency of the emitted light coincides with the transition frequency of the semiconductor medium, whereas at $\delta < 0$ the lasing frequency follows the variation in the cavity length. This agrees with the dispersive mechanism of the spatial structure formation. Since in our system the depth and the position of the lasing threshold minimum are also mainly determined by the detuning δ, we observe a similar behaviour. Fig. 7

shows the dependence of the lasing frequency on the cavity length. One can see that at $\delta < 0$ ($\Delta L/L < 0$) the lasing frequency follows the cavity frequency, whereas at $\Delta L/L > 0.0005$ it coincides with the transition frequency. The deviation from this behaviour in the narrow interval $0.0005 > \Delta L/L > 0$ is due to the Bragg dispersion mechanism, which is not completely suppressed by the Lorentzian profile in this interval.

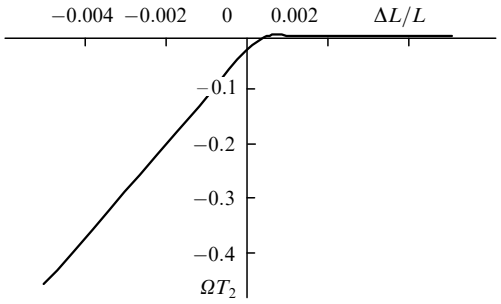

Figure 7. Dependence of the frequency shift, Ω, on the change in the resonator length, ΔL. Ω and ΔL are shown in relative units.

Thus, we have shown in this work that the selection of spatial Fourier modes in a wide-aperture VCSEL can be a result of the well-known gain dispersion mechanism as well as of the reflection coefficient dispersion of the Bragg mirrors of the laser cavity. The first dispersion mechanism primarily determines the position and the depth of the lasing threshold minimum for spatial harmonics, whereas the Bragg dispersion mechanism gives rise to an anisotropy of spatial dependence of the lasing threshold. The lowest threshold corresponds to spatial harmonics whose wave vector is perpendicular to the polarisation of the emission.

The gain dispersion considerably depends on the position of the active layer inside the cavity. This is due to the dependence of the phase incursion in various parts of the cavity, which determines the frequency shifts of the spatial harmonics, on the longitudinal dimension of these parts. The two selection mechanisms can either suppress or enhance each other, leading to more or less pronounced selection of spatial harmonics.

The results of the numerical simulation show stationary transverse structures appearing near the lasing threshold. These are stripes parallel to the polarisation vector of the emission. The analysis of higher pump intensities requires considering the vector nature of the emission field as well as a more adequate description of the interaction between the semiconductor medium and radiation.

Acknowledgements. This work was supported by Belarussian Republic Foundation for Basic Research.

References

1. Vertical-Cavity Surface-Emitting Lasers *Proc. SPIE* **3003** (1997)
2. Huyet G, Martinoni M C, Treddice J R, Rica S *Phys. Rev. Lett.* **75** 4027 (1995)
3. Coullet P, Gil L, Rocca F *Opt. Commun.* **73** 403 (1989)
4. Lugiato L A, Oppo J R, Treddice J R, Narducci L M, Pernigo M A *J. Opt. Soc. Am. B* **7** 1019 (1990)
5. Jakobsen P K, Moloney J V, Newell A C, Indik R *Phys. Rev. A* **45** 8129 (1992)
6. Staliunas K, Weiss C O *Physica D* **81** 79 (1995)
7. Brambilla M, Lugiato L A, Prati F, Spinelli L, Firth W J *Phys. Rev. Lett.* **79** 2042 (1997)
8. Hegarty S P, Huyet G, McInerney J G, Hou H Q, Choquette K D *Phys. Rev. Lett.* **82** 1434 (1999)
9. Chang-Hasnain C J, Harbison J P, Hasnain G, von Lehmen A, Florez L T, Stoffel N G *IEEE J. Quantum Electron.* **27** 1402 (1991)
10. Choquette K D, Richie D A, Leibenguth R E *Appl. Phys. Lett.* **64** 2062 (1994)
11. Oraevskii A N *Kvantovaya Elektron.* **19** 979 (1992) [*Sov. J. Quantum Electron.* **22** 910 (1992)]
12. Logvin Yu A, Loiko N A, Turovets S I, Spencer P S, Shore K A *Laser Physics* **7** 1160 (1997)
13. Benedict M, Malyshev V A, Trifonov E D et al. *Phys. Rev. A* **43** 3845 (1991)
14. Born M, Wolf E *Principles of Optics* (New York: Pergamon, 1980; Moscow: Nauka, 1973)
15. Babic D J, Dagli Yo, Chung N, Bowers J E *IEEE J. Quantum Electron.* **29** 1950 (1993)
16. Ebeling K J *SUSSP Proc.* **50** 295 (1998)
17. Chow W W, Koch S W, Sargent M III *Semiconductor Laser Physics* (New York: Springer, 1994)
18. Ning C Z, Indik R A, Moloney J V *IEEE J. Quantum Electron.* **33** 1543 (1997)
19. Walgraef D *Spatio-Temporal Pattern Formation* (New York: Springer, 1997)